

SFU HEP-152-98

Tadpole-improved SU(2) lattice gauge theory

Norman H. Shakespeare* and Howard D. Trottier†

Department of Physics, Simon Fraser University, Burnaby, B.C., Canada V5A 1S6
(March 1998)

Abstract

A comprehensive analysis of tadpole-improved SU(2) lattice gauge theory is made. Simulations are done on isotropic and anisotropic lattices, with and without improvement. Two tadpole renormalization schemes are employed, one using average plaquettes, the other using mean links in Landau gauge. Simulations are done with spatial lattice spacings a_s in the range of about 0.1–0.4 fm. Results are presented for the static quark potential, the renormalized lattice anisotropy a_t/a_s (where a_t is the “temporal” lattice spacing), and for the scalar and tensor glueball masses. Tadpole improvement significantly reduces discretization errors in the static quark potential and in the scalar glueball mass, and results in very little renormalization of the bare anisotropy that is input to the action. We also find that tadpole improvement using mean links in Landau gauge results in smaller discretization errors in the scalar glueball mass (as well as in the static quark potential), compared to when average plaquettes are used. The possibility is also raised that further improvement in the scalar glueball mass may result when the coefficients of the operators which correct for discretization errors in the action are computed beyond tree level.

Typeset using REVTeX

*Email address: nshakesp@sfu.ca.

†Email address: trottier@sfu.ca.

I. INTRODUCTION

Simulations of lattice Quantum Chromodynamics (QCD) have undergone significant changes in the past few years, with a host of new actions under investigation, and with the viewpoint emerging that simulations on coarse lattice can yield reliable results. A major impetus for these changes was the realization that the large radiative corrections which occur in many quantities in lattice theories have a common origin, coming from cutoff effects due to tadpole diagrams specific to lattice actions [1].

Tadpole diagrams in lattice theories are induced by the nonlinear connection between the lattice link variables $U_\mu(x)$ and the continuum gauge fields $A_\mu(x)$,

$$U_\mu(x) \equiv e^{i a g A_\mu(x)}. \quad (1)$$

The cutoff dependence of ultraviolet divergent tadpole diagrams spoils naive power counting in the lattice spacing a . Higher dimension operators that are generated by lattice actions generally induce large radiative corrections, their contributions being suppressed by powers of $\alpha_s(a)$, rather than of a . Fortunately, there is now considerable evidence that the effects of tadpole diagrams can largely be removed with a simple mean field renormalization of the links [1]

$$U_\mu(x) \rightarrow \frac{U_\mu(x)}{u_0}, \quad (2)$$

where an operator dominated by short-distance fluctuations is used to determine u_0 . (Alternative approaches to the design of improved lattice actions include the construction of fixed point actions [2], and the use of nonperturbative renormalization conditions [3].)

Tadpole improvement has helped to revitalize interest in the Symanzik improvement program [4], with a number of new more complex actions currently under investigation, partly with the goal of doing precision simulations on coarse lattices (for a review see Ref. [5]). One of the earliest applications of tadpole improvement was in the development of the nonrelativistic QCD (NRQCD) action for heavy quarks [6]. Tadpole improvement is now widely used in large scale simulations of many actions [7], and plays an important role in current efforts to extract continuum results from simulations on fine lattices.

The current interest in simulations on very coarse lattices was stimulated by the first study of tadpole-improved gluonic actions [8]. Simulations of the static quark potential, and of the spin-average charmonium spectrum in NRQCD, using an improved gluonic action on lattices with spacings as large as 0.4 fm, showed discretization errors of only a few percent.

This has led to more recent efforts to further optimize tadpole-improved actions. In particular, there has been considerable work to determine the optimal choice of operator to use in defining the mean field renormalization factor u_0 [9–13]. Most previous simulations have used the fourth root of the average plaquette $u_{0,P}$ for tadpole improvement where, in $SU(N)$ gauge theory (on isotropic lattices)

$$u_{0,P} \equiv \left\langle \frac{1}{N} \text{ReTr } U_{\text{pl}} \right\rangle^{1/4}. \quad (3)$$

However simulations of the static quark potential [9], of the quarkonium spectrum in NRQCD [10,12,13], and of a relativistic fermion action [11] have demonstrated that discretization errors are further reduced when the mean link in Landau gauge $u_{0,L}$ is used, where

$$u_{0,L} \equiv \left\langle \frac{1}{N} \text{ReTr} U_\mu \right\rangle, \quad \partial_\mu A_\mu = 0. \quad (4)$$

There has also been a rapid evolution of more complex, highly improved actions (see e.g. Refs. [5,11,14,15]). In particular, there has been a revival of interest in actions defined on anisotropic lattices, where the lattice spacing in the “temporal” direction a_t is kept smaller than the spatial spacing a_s [14,15]. This enables much more efficient simulations of hadronic systems with large masses, for example, where the exponential suppression of the correlation function becomes prohibitive on lattices with large a_t . This is especially relevant for glueball simulations, where discretization errors may be acceptably small even with a_s as large as 0.4 fm [16–18], but where the correlation function becomes extremely noisy after only a few time steps if a comparable a_t is used.

An impediment to the use of anisotropic lattices has been the need to measure the renormalized anisotropy $(a_t/a_s)_{\text{phys}}$ in the simulation which, in the case of the Wilson gluon action [19,20], can differ appreciably from the bare anisotropy ξ that is input to the action

$$\xi \equiv \left(\frac{a_t}{a_s} \right)_{\text{bare}}. \quad (5)$$

However it has recently been shown that tadpole improvement reduces the renormalization of ξ to a few percent [14,15], which is small enough to be neglected in many applications. Recent simulations of a variety of glueball states with a tadpole-improved action, on anisotropic lattices with coarse a_s , have provided results that compete with much larger scale simulations on fine lattices [17,18].

In this paper we present a comprehensive analysis of the tadpole-improved SU(2) lattice gauge theory. We do simulations on both isotropic and anisotropic actions, with and without improvement. Results are obtained with two tadpole renormalization schemes, one using average plaquettes, and the other using mean links in Landau gauge. We also compare with simulations of the Wilson action. Simulations are done with spatial spacings a_s in the range of about 0.1–0.4 fm. Results are presented for the static quark potential, the renormalized anisotropy, and for the scalar and tensor glueball masses. Some of our results have been reviewed in preliminary form elsewhere [5,14,15,18]. A full account of this work is presented here for the first time [21]. (Simulations of the tadpole-improved SU(2) gauge theory on isotropic lattices have also recently been reported in Refs. [22,23].)

We note that there is a long history of simulations of SU(2) gauge theory, motivated by the fact that this theory exhibits much of the physics found in SU(3) color, including linear confinement of static quarks and a rich glueball spectrum. Simulations of SU(2) color have been used to shed light on the physics of confinement, and to test new algorithms for use in more realistic simulations. The reduced computational cost of simulations in SU(2) continues to be exploited in, for example, recent large scale simulations of the static quark potential [24].

The work we present here on tadpole-improved SU(2) gluonic actions is not only of interest in reproducing the features of the SU(3) theory, but also serves to suggest new avenues for further development. Of particular interest are new results presented here for the SU(2) scalar glueball mass, which relate to a peculiar feature that has previously been observed in SU(3) coarse lattice simulations [17]. We find that the SU(2) scalar glueball mass first decreases as the lattice spacing a_s is increased, reaching a minimum at $a_s \approx 0.3$ fm; the

mass then gradually increases with a_s . A similar “dip” in the SU(3) scalar glueball mass was reported in Ref. [17]. It has been conjectured [17,18] that this behavior may be related to the presence of a critical endpoint in a line of phase transitions in gluonic actions that include an adjoint coupling [25].

On the other hand, we find that the depth of the dip in the SU(2) theory with plaquette tadpole improvement is about half of that found with the Wilson action. We also find that the depth of the dip is further reduced when mean link tadpole improvement is used (the SU(3) simulations in Ref. [17] were done with average plaquette tadpoles). This suggests that the dip may be due, at least in part, to discretization errors that are more fully removed with mean link tadpoles. The tensor glueball mass exhibits relatively small scaling violations even with the Wilson action, which could indicate that the tensor has a larger size than the scalar. In this connection, we note that the scalar glueball has been found to be much less sensitive to finite volume effects than the tensor [26]. This supports the conjecture that the scalar glueball has a smaller size than the tensor, and hence is more sensitive to discretization corrections to the action.

We also performed simulations after making small changes to the coefficients of the operators which correct for discretization errors in the action. These results raise the possibility that the dip in the scalar glueball mass might be eliminated once the correct $O(\alpha_s)$ renormalizations of the relevant operators in the action are included.

The rest of this paper is organized as follows. In Sect. II we present results from an improved SU(2) action on isotropic lattices. Two independent sets of simulations are done, using the two tadpole renormalization schemes discussed above (Eqs. (3) and (4)). We simulate on lattices with spacings of about 0.25 fm and 0.40 fm. We compare the static quark potential with improvement to the results of a simulation using the Wilson action. We also present results for the scalar glueball mass. Details of our Wilson loop and glueball correlation functions are also discussed in Sect. II.

In Sect. III we present results from our simulations on anisotropic lattices. We run at several spatial lattice spacings a_s in the range of about 0.1 fm to 0.4 fm, where the temporal spacing a_t is kept near 0.1 fm. We run simulations for improved actions using the two tadpole renormalization schemes, and we also run on several lattices using the Wilson action. We compare bare and renormalized anisotropies, static quark potentials, and scalar and tensor glueball masses from these actions. We also illustrate the sensitivity of the scalar glueball mass to small changes in the coefficients of the operators which correct for discretization errors in the action. We briefly summarize our results and outline possible directions for further work in Sect. IV.

II. ISOTROPIC LATTICES

The isotropic tadpole-improved action for SU(2) is identical in form to the SU(3) action [8], and at tree level is given by

$$\mathcal{S} = -\beta \sum_{x, \mu > \nu} \left\{ \frac{5}{3} \frac{P_{\mu\nu}}{u_0^4} - \frac{1}{12} \frac{R_{\mu\nu}}{u_0^6} - \frac{1}{12} \frac{R_{\nu\mu}}{u_0^6} \right\}, \quad (6)$$

where $P_{\mu\nu}$ is one half the trace of the 1×1 Wilson loop in the $\mu \times \nu$ plane, and $R_{\mu\nu}$ is one half the trace of the 2×1 rectangle in the $\mu \times \nu$ plane. The notation used in Eq. (6)

differs slightly from that used in Ref. [8], where a factor of $5/3u_0^4$ was absorbed into the definition of β . The notation used here follows that introduced in Refs. [14,15]. The leading discretization errors in this action are of $O(\alpha_s a^2)$ and $O(a^4)$.

We ran simulations at two lattice couplings using plaquette improvement, $u_0 = u_{0,P}$ (Eq. (3)), and at one lattice coupling using mean link improvement, $u_0 = u_{0,L}$ (Eq. (4)). For comparison, results were also obtained for a standard Wilson action on a coarse lattice. The parameters of these four lattices are given in Table I. In the following we will use β_P and β_L to denote the lattice couplings for the improved action with plaquette and mean link tadpoles respectively, and β_W for the Wilson action coupling.

Results for the static quark potential $V(R)$ on the lattices with comparable spacings are shown in Fig. 1. The potentials were measured at integer separations $R/a = 1\text{--}4$. Measurements were also made using non-planar Wilson loops, corresponding to separations $R/a = \sqrt{2}, \sqrt{3}, \sqrt{5}$, and $\sqrt{8}$. Symmetric combinations of the shortest spatial paths connecting two lattice points were used in the non-planar Wilson loop calculations. The data in Fig. 1 were obtained by looking for a plateau in the time-dependent effective potential

$$aV(R, T) = -\ln \left[\frac{W(R, T)}{W(R, T-1)} \right], \quad (7)$$

where $W(R, T)$ denotes the Wilson loop. An estimate of the systematic error in the large T extrapolation is given by the statistical error in the second or third time step after the onset of the plateau.

An iterative fuzzing procedure was used to construct Wilson loop (and glueball) operators with a very high degree of overlap with the lowest-lying state. Fuzzy link variables $U_i^{(n)}(x)$ at the n th step of the iteration were obtained from a linear combination of the link and surrounding staples from the previous step [27]

$$U_i^{(n)}(x) = U_i^{(n-1)}(x) + \epsilon \sum_{j \neq \pm i} U_j^{(n-1)}(x) U_i^{(n-1)}(x + \hat{j}) U_j^{(n-1)\dagger}(x + \hat{i}), \quad (8)$$

where i and j are purely spatial indices, and where the links were normalized to $U^\dagger U = I$ after each iteration. Wilson loops (and glueball correlators, Eq. (12) below) were constructed as usual by using the fuzzy link variables in place of the original links. The optimal number of iterations n and the parameter ϵ typically varied from $(n, \epsilon) = (10, 0.04)$ on lattices with $a \approx 0.4$ fm to $(n, \epsilon) = (5, 0.4)$ on lattices with $a \approx 0.1$ fm.

A defect of the action Eq. (6) is that the gluon propagator acquires a high energy pole with a negative residue (at least in perturbation theory), due to terms in the action with two links in the time direction [14,15]. One consequence of these high energy ‘‘doublers’’ is that correlation functions exhibit exponential decay only at sufficiently large times. This is illustrated by an increase in the time-dependent potential $V(R, T)$ at small times, as shown in Fig. 2. This complicates the extraction of masses on coarse isotropic lattices, given the severe suppression of the correlation function at large times. This problem can be avoided by working on anisotropic lattices with sufficiently small a_t , where elimination of $O(a_t^2)$ errors in the action may be unnecessary, as described in the next section.

The solid lines in Fig. 1 show the results of a fit of the on-axis data to a standard infrared parameterization of the continuum potential:

$$V_{\text{fit}}(R) = \sigma R - \frac{b}{R} + c. \quad (9)$$

Infrared fluctuations of a one-dimensional string give $b = \pi/12$ [28]. However much better fits were obtained by leaving b as a free parameter. We typically found $b \approx 0.1$ on the coarsest lattices, with the string value emerging on the finest lattices analyzed in Sect. III (see also Ref. [17]). The lattice spacings a were extracted by matching the fit values for the string tension in lattice units to a physical value of $\sqrt{\sigma} = 0.44$ GeV.

Discretization errors in the lattice action break Lorentz symmetry, which is clearly visible in the off-axis potentials [8]. These errors are dramatically reduced when the action is tadpole improved, as seen in Fig. 1. As a quantitative measure of the improvement, we compare the potential measured in the simulation from non-planar Wilson loops with an interpolation to the on-axis data:

$$\Delta V(R) \equiv \frac{V_{\text{sim}}(R) - V_{\text{fit}}(R)}{\sigma R}. \quad (10)$$

Results for $R = (a, a, a)$ are given in Table I. With tadpole improvement the error is only a few percent even on lattices with spacings as large as 0.4 fm, compared to an error of about 30–40% for the Wilson action [8]. Discretization errors are further reduced when tadpole improvement is done with $u_{0,L}$, compared to when $u_{0,P}$ is used.

Glueball correlation functions $G(T)$ were also calculated

$$G(T) = \langle \phi(T) \phi(0) \rangle - \langle \phi \rangle^2, \quad (11)$$

where $\phi(T)$ denotes a linear combination of the trace of 1×1 (fuzzy) plaquettes $P_{ij}(\vec{x}, T)$, summed over spatial positions. We considered linear combinations which, in the continuum limit, excite scalar ($J^P = 0^+$) and tensor ($J^P = 2^+$) glueballs:

$$\begin{aligned} \phi_{0+}(T) &= \sum_{\vec{x}} [P_{12}(\vec{x}, T) + P_{13}(\vec{x}, T) + P_{23}(\vec{x}, T)], \\ \phi_{2+}(T) &= \sum_{\vec{x}} [P_{12}(\vec{x}, T) - P_{13}(\vec{x}, T)], \end{aligned} \quad (12)$$

together with two other linearly independent combinations of plaquettes for the tensor channel. Effective masses $m(T)$ were computed in the usual way:

$$m(T) = -\ln \left(\frac{G(T)}{G(T-1)} \right). \quad (13)$$

An effective mass plot for the scalar glueball on the improved lattice with $a \approx 0.26$ fm is shown in Fig. 3. The data are very noisy even at T of two or three lattice units, due to the large lattice spacing and glueball mass, despite the fact that an ensemble of over 30,000 configurations was generated. The data for the tensor glueball were too noisy to be of use. As with the SU(3) simulations reported in Ref. [16], the extraction of the glueball mass from a plateau in $m(T)$ is computationally demanding on coarse isotropic lattices. As shown in the next section a far more efficient approach, proposed in Refs. [14,15], is to simulate on anisotropic lattices with small spacings in the time direction. On the other hand, the results in Fig. 3 compare favorably with Wilson action calculations on fine lattices [29]. In Ref. [30] a continuum extrapolation of Wilson action glueball data was made, with the result $m_{0+}/\sqrt{\sigma} = 3.87 \pm 0.12$.

III. ANISOTROPIC LATTICES

The tadpole-improved SU(2) action on anisotropic lattices is again identical in form to the SU(3) theory and, following Refs. [14,15], we omit corrections for $O(a_t^2)$ errors by working on lattices with small a_t . This has the advantage of eliminating a negative residue high energy pole in the gluon propagator. The resulting action has rectangles R_{st} that extend only one lattice spacing in the time direction:

$$\begin{aligned} \mathcal{S} = & -\beta \sum_{x,s>s'} \xi \left\{ \frac{5}{3} \frac{P_{ss'}}{u_s^4} - \frac{1}{12} \frac{R_{ss'}}{u_s^6} - \frac{1}{12} \frac{R_{s's}}{u_s^6} \right\} \\ & -\beta \sum_{x,s} \frac{1}{\xi} \left\{ \frac{4}{3} \frac{P_{st}}{u_s^2 u_t^2} - \frac{1}{12} \frac{R_{st}}{u_s^4 u_t^2} \right\}, \end{aligned} \quad (14)$$

where ξ is the bare anisotropy, Eq. (5). “Diagonal” correlation functions computed from this action decrease monotonically with time.

On an anisotropic lattice one has two mean fields u_t and u_s . A natural way to determine them is to use the mean links in Landau gauge [5]

$$u_t = \left\langle \frac{1}{2} \text{ReTr } U_4 \right\rangle, \quad u_s = \left\langle \frac{1}{2} \text{ReTr } U_s \right\rangle, \quad (15)$$

where a lattice version of the continuum Landau gauge condition $\partial_\mu A_\mu = 0$ is obtained by maximizing the quantity

$$\sum_{x,\mu} \frac{1}{u_\mu a_\mu^2} \text{ReTr } U_\mu(x). \quad (16)$$

Alternatively one can define the mean fields using the measured values of the average plaquettes. One possibility is to first compute u_s from spatial plaquettes, $u_s^4 = P_{ss'}$, and then to compute u_t from temporal plaquettes, $u_t^2 u_s^2 = P_{st}$. However, in the limit that $a_t/a_s \rightarrow 0$, this procedure yields $u_t \rightarrow 1/u_s$ [31]; with mean link tadpoles Eq. (15) on the other hand one has the more physical limit $u_t = 1 - O((a_t/a_s)^2)$. Since the lattice spacing a_t in our simulations is small, we adopt the following prescription [14,15,17] for the mean fields in “plaquette improvement”

$$u_t \equiv 1, \quad u_s = \langle P_{ss'} \rangle^{1/4}. \quad (17)$$

In this connection, we note that the factor u_t in the action Eq. (14) can in fact be absorbed into a redefinition of β and of the input anisotropy, according to $\beta/u_t \rightarrow \beta$, and $\xi u_t \rightarrow \xi$. As shown below one finds very little renormalization of the input anisotropy ξ with either of the tadpole renormalization schemes Eqs. (15) or (17).

Simulations were performed on four lattices with plaquette improvement, and three lattices with mean link tadpoles. In addition, we ran simulations on six lattices with the Wilson action. The parameters of these thirteen lattices are given in Table II. The spatial spacings a_s lie in the range of about 0.1 fm to 0.4 fm, with temporal spacings a_t kept near 0.1 fm.

Configurations were generated using a heat bath algorithm. The number of updates between measurements varied from 10 on the coarsest lattices to 20 on the finest; integrated autocorrelation times were computed, and satisfied $\tau_{\text{int}} \lesssim 0.5$ in all cases. Ensembles of

about 2,000 configurations were used to measure the static quark potential, while between 80,000 and 160,000 configurations were generated at each β for glueball measurements.

Tadpole improvement eliminates most of the renormalization of the input anisotropy ξ , as was first shown in Refs. [14,15]. This can be demonstrated by comparing the static quark potential computed from Wilson loops W_{xt} , where the time axis is taken in the direction of small lattice spacings a_t ,

$$W_{xt}(R = n_1 a_s, T = n_2 a_t) \xrightarrow{n_2 \rightarrow \infty} Z_{xt} e^{-n_2 a_t V(R)}, \quad (18)$$

with the potential computed from Wilson loops W_{xy} with both axes taken in the direction of large lattice spacings a_s

$$W_{xy}(R = n_1 a_s, T = n_2 a_s) \xrightarrow{n_2 \rightarrow \infty} Z_{xy} e^{-n_2 a_s V(R)}. \quad (19)$$

The physical anisotropy is determined after an unphysical constant is removed from the potentials, by subtraction of the simulation results at two different radii

$$\left(\frac{a_t}{a_s}\right)_{\text{phys}} = \frac{a_t V_{xt}(R_2) - a_t V_{xt}(R_1)}{a_s V_{xy}(R_2) - a_s V_{xy}(R_1)}, \quad (20)$$

where $a_t V_{xt}$ and $a_s V_{xy}$ are the potentials in the lattice units relevant to the two sets of Wilson loops W_{xt} and W_{xy} , respectively (alternative methods for determining the renormalized anisotropy are analyzed in Ref. [20]).

We computed the anisotropy twice, using two different radii R_1 for the subtraction, with fixed $R_2 = 2a_s$. We compare the anisotropies determined with $R_1 = a$ and $\sqrt{2}a$ in Table III. Although it is advantageous to use the potential at smaller R , where the statistical errors are smaller, it is important to check that we are not sensitive to possible discretization errors of $O(a_s^4/R^4)$ [31]. The two determinations of the anisotropy are in fact in excellent agreement.

These results show that the input anisotropy ξ is renormalized by less than a few percent when the action is tadpole improved [14,15], at least over the wide range of lattices analyzed here. The renormalization is small enough that one need not measure the anisotropy in many applications. This is to be contrasted with the Wilson action, where the measured value of a_t/a_s is found to be about 20% lower than ξ on the lattices analyzed here.

Sample results for the potentials both with and without tadpole improvement are shown in Fig. 4. The renormalization of the input anisotropy in the case of the Wilson action is plainly visible as a difference in slope of the potentials computed from W_{xt} and W_{xy} . A significant reduction in rotational symmetry breaking with the improved action is also apparent in the off-axis potentials, as illustrated in Fig. 4.

The scalar and tensor glueball correlators were calculated on all thirteen lattices. Representative effective mass plots are shown in Fig. 5. The fuzzy correlators described in Sect. II (Eqs. (8) and (12)) were used. We note that the efficiency of these calculations could be improved by using a variational basis of several operators, rather than just the fuzzy 1×1 plaquette used here [17]. Our final results for the masses were obtained from single exponential fits to the correlation functions. In most cases acceptable fit results for the scalar glueball were obtained from the fit interval $T = (3-5)a_t$ (we required that these fits be in good agreement with fits using larger intervals in T). The results are given in Table IV.

The scalar and tensor glueball masses are shown as functions of lattice spacing squared in Figs. 6 and 7. The tensor glueball data exhibit relatively small scaling violations, even

for the Wilson action on the coarsest lattices studied here. This could indicate that the tensor glueball has a very large size. It would be interesting to compare with the situation for the SU(3) tensor glueball, but Wilson action data are not available on sufficiently coarse lattices (for a compilation see Ref. [17]).

The SU(2) scalar glueball data exhibit a peculiar feature that has previously been observed in SU(3) coarse lattice simulations [17]. The scalar glueball mass first decreases as a_s increases, reaching a minimum at $a_s \approx 0.3$ fm; the mass then gradually increases with a_s . It has been conjectured [17,18] that this “dip” may be related to the presence of a critical endpoint in a line of phase transitions in gluonic actions that include an adjoint coupling [25].

The data obtained here shed new light on this behavior. In particular, we find that the depth of the dip is reduced by about half when the plaquette-improved action is used, compared to results obtained with the Wilson action. We also find that the depth of the dip is further reduced when mean link improvement is used. This suggests that the dip may be due, at least in part, to discretization errors that are more fully removed with mean link tadpoles.

We note that the SU(3) simulations in Ref. [17] were done with plaquette improvement. The SU(3) scalar glueball dip is more pronounced than in SU(2) with plaquette improvement, but Wilson action data are not available on sufficiently coarse lattices to allow a trend to be established in the SU(3) theory. Simulations with mean link improvement for SU(3) glueballs have not been done. On the other hand, some SU(3) simulations have been done with an adhoc change to the action, designed to move the theory away from the critical endpoint in the fundamental-adjoint plane [18]; these results suggest that this mechanism does play a role in the SU(3) scalar glueball dip.

In this connection we performed one last set of simulations, after making an adhoc change to the coefficient of the rectangle terms $R_{ss'}$ and R_{st} in Eq. (14). We multiplied these terms by a factor of 1.2, which is consistent with an $O(\alpha_s)$ renormalization of these operators on lattices with spacings in the range considered here. We ran at $\beta_L = 0.85$, with $\xi = 0.333$ (after retuning the Landau gauge mean link factors, where $u_t = 0.975$ and $u_s = 0.758$). The lattice spacing $a_s = 0.314(1)$ fm is in the middle of the dip found with the other actions. We find glueball masses $m_{0+}/\sqrt{\sigma} = 3.82(7)$, and $m_{2+}/\sqrt{\sigma} = 5.5(4)$ (where a measured renormalization of ξ by about 8% is included). These results are shown as an open triangle in Fig. 6 and 7. These results raise the possibility that the dip in the scalar glueball mass might be eliminated once the correct $O(\alpha_s)$ renormalizations of the operators which correct for discretization errors in the action are included. This conjecture is supported by finite volume studies of the glueball spectrum, which show that the scalar is much less sensitive to finite volume effects than the tensor [26].

IV. SUMMARY AND OUTLOOK

Tadpole improved SU(2) lattice gauge theory was applied to calculations of the heavy quark potential, the renormalized lattice anisotropy, and the scalar and tensor glueball masses. We analyzed improved actions on isotropic and anisotropic lattices, and we compared simulations with mean link and plaquette tadpole improvement. Comparisons were also made with simulations of the Wilson action. Tadpole improvement significantly reduces

discretization errors in the static quark potential, and results in very little renormalization of the input anisotropy. We also found a “dip” structure in the scalar glueball mass, analyzed as a function of lattice spacing, which has previously been observed in SU(3) simulations. We found evidence that this dip may be related to discretization errors in the action that are more fully removed when tadpole improvement is done using the mean link in Landau gauge. The possibility was also raised that further improvement in the scalar glueball mass may result when the coefficients of the operators which correct for discretization errors in the action are computed beyond tree level.

Simulations with mean link improvement (as well as of the Wilson action) on coarse lattices in the SU(3) theory could help to clarify the origin of the dip in the scalar glueball mass. It might also be fruitful to analyze an improved SU(2) theory with an adjoint coupling included. A calculation of the scalar and tensor glueball sizes would also yield useful information, with the reduced computational cost of simulations in the SU(2) gauge theory providing further incentive for continued study of this system.

ACKNOWLEDGMENTS

We thank C. Morningstar, M. Peardon, and R. M. Woloshyn for helpful conversations. We are especially indebted to G. P. Lepage for numerous suggestions and discussions which provided the impetus for much of this work. This work was supported in part by the Natural Sciences and Engineering Research Council of Canada.

REFERENCES

- [1] G. P. Lepage and P. B. Mackenzie, Phys. Rev. D **48**, 2250 (1993).
- [2] For a review see F. Niedermayer, Nucl. Phys. B (Proc. Suppl.) **53**, 56 (1997).
- [3] For a review see M. Lüscher, Report No. hep-lat/9802029.
- [4] K. Symanzik, Nucl. Phys. B **226**, 187 (1983); M. Lüscher and P. Weisz, Commun. Math. Phys. **97**, 59 (1985).
- [5] G. P. Lepage, Nucl. Phys. A (Proc. Suppl.) **60**, 267 (1998).
- [6] For a review see C. T. H. Davies, Report No. hep-ph/9710394.
- [7] For a recent review of work on light hadron spectroscopy see e.g. T. Yoshié, Report No. hep-lat/9711017.
- [8] M. Alford, W. Dimm, G. P. Lepage, G. Hockney, and P. B. Mackenzie, Nucl. Phys. B (Proc. Suppl.) **42**, 787 (1995); Phys. Lett. B **361**, 87 (1995).
- [9] M. G. Alford, T. R. Klassen and G. P. Lepage, unpublished. See also Ref. [5].
- [10] H. D. Trottier, Phys. Rev. D **55**, 6844 (1997).
- [11] M. G. Alford, T. R. Klassen and G. P. Lepage, Report No. hep-lat/9712005.
- [12] N. H. Shakespeare and H. D. Trottier, Report No. hep-lat/9802038.
- [13] C. T. H. Davies *et al.*, NRQCD Collaboration, Report No. hep-lat/9802024.
- [14] M. Alford, T. R. Klassen, G. P. Lepage, C. J. Morningstar, and M. Peardon (unpublished).
- [15] C. J. Morningstar, Nucl. Phys. B (Proc. Suppl.) **53**, 914 (1997).
- [16] C. J. Morningstar and M. Peardon, Nucl. Phys. B (Proc. Suppl.) **47**, 258 (1996).
- [17] C. J. Morningstar and M. Peardon, Phys. Rev. D **56**, 4043 (1997); Nucl. Phys. B (Proc. Suppl.) **53**, 917 (1997);
- [18] M. Peardon, Report No. hep-lat/9710029.
- [19] See e.g. G. Burgers, F. Karsch, A. Nakamura, and I. O. Stamatescu, Nucl. Phys. B **304**, 587 (1988).
- [20] T. R. Klassen, Report No. hep-lat/9803010.
- [21] Some of this work was reported in unpublished form in N. H. Shakespeare, M.Sc. thesis, Simon Fraser University (1996).
- [22] G. I. Poulis, Phys. Rev. D **56**, 161 (1997).
- [23] P. Pennanen and J. Peisa, Report No. hep-lat/9709048.
- [24] See e.g. S. P. Booth *et al.*, UKQCD Collaboration, Nucl. Phys. B **394**, 509 (1993); G. S. Bali, K. Schilling, and C. Schlichter, Phys. Rev. D **51**, 5165 (1995).
- [25] A. Patel *et al.*, Phys. Rev. Lett. **57**, 1288 (1986); U. Heller, Phys. Lett. B **362**, 123 (1995).
- [26] For a review of finite volume studies of glueball masses see P. van Baal and A. S. Kronfeld, Nucl. Phys. B (Proc. Suppl.) **9**, 227 (1989).
- [27] M. Albanese *et al.*, Phys. Lett. B **192**, 163 (1987).
- [28] M. Lüscher, K. Symanzik, and P. Weisz, Nucl. Phys. B **173**, 365 (1980).
- [29] C. Michael and M. Teper, Phys. Lett. B **199**, 95 (1987); Nucl. Phys. B **305**, 453 (1988); C. Michael and S. J. Perantonis, J. Phys. G **18**, 1725 (1992).
- [30] T. Moretto and M. Teper, Report No. hep-lat/9312035.
- [31] G. P. Lepage, private communication.

TABLES

| Action | β | $\langle \frac{1}{3} \text{ReTr } U_{\text{pl}} \rangle^{1/4}$ | $\langle \frac{1}{3} \text{ReTr } U_{\mu} \rangle^{1/4}$ | a (fm) | Volume | $\Delta V(\sqrt{3}a)$ |
|-------------------------|---------|--|--|----------|--------|-----------------------|
| Improved (Plaquette) | 0.730 | 0.844 | 0.779 | 0.394(2) | 8^4 | 0.04(1) |
| | 0.935 | 0.872 | 0.817 | 0.264(1) | 8^4 | 0.02(1) |
| Improved (Landau) | 0.550 | 0.845 | 0.779 | 0.404(2) | 8^4 | 0.01(1) |
| | Wilson | 1.700 | 0.802 | 0.402(2) | 8^4 | 0.32(4) |

TABLE I. Simulation parameters for three isotropic tadpole-improved lattices, and one Wilson action lattice. The mean field for plaquette improvement (second column) and mean link improvement (third column) are given. The lattice spacings were determined from the string tension, with $\sqrt{\sigma} = 0.44$ GeV. The measured errors ΔV in the off-axis potential at $R = (a, a, a)$ are also shown (see Eq. (10)).

| Action | β | ξ | u_t | u_s | a (fm) | Volume |
|-------------------------|---------|-------|-------|-------|----------|------------------|
| Improved (Plaquette) | 0.848 | 0.276 | 1. | 0.793 | 0.366(1) | $8^3 \times 32$ |
| | 0.981 | 0.333 | 1. | 0.819 | 0.298(1) | $8^3 \times 24$ |
| | 1.114 | 0.409 | 1. | 0.842 | 0.238(1) | $8^3 \times 20$ |
| | 1.214 | 0.500 | 1. | 0.860 | 0.202(2) | $10^3 \times 20$ |
| Improved (Landau) | 0.650 | 0.276 | 0.977 | 0.718 | 0.384(2) | $8^3 \times 32$ |
| | 0.795 | 0.333 | 0.974 | 0.757 | 0.304(1) | $8^3 \times 24$ |
| | 0.905 | 0.409 | 0.966 | 0.785 | 0.244(1) | $8^3 \times 20$ |
| Wilson | 1.950 | 0.250 | | | 0.393(2) | $8^3 \times 32$ |
| | 2.000 | 0.250 | | | 0.355(2) | $8^3 \times 32$ |
| | 2.140 | 0.333 | | | 0.308(2) | $8^3 \times 24$ |
| | 2.243 | 0.400 | | | 0.232(2) | $8^3 \times 20$ |
| | 2.300 | 0.500 | | | 0.203(1) | $10^3 \times 20$ |
| | 2.400 | 1. | | | 0.128(2) | 12^4 |

TABLE II. Simulation parameters for the lattices analyzed in Sect. III. The bare anisotropies ξ and the mean fields u_t and u_s for tadpole improvement are shown, along with the spatial lattice spacings a_s determined from the string tension.

| Action | β | ξ | $(a_t/a_s)_{\text{phys}}$ $(R_1 = a_s)$ | $(a_t/a_s)_{\text{phys}}$ $(R_1 = \sqrt{2}a_s)$ | $\Delta V(\sqrt{3}a)$ |
|-------------------------|---------|-------|--|--|-----------------------|
| Improved (Plaquette) | 0.848 | 0.276 | 0.273(4) | 0.272(8) | 0.08(1) |
| | 0.981 | 0.333 | 0.335(5) | 0.332(10) | 0.05(1) |
| | 1.114 | 0.409 | 0.413(3) | 0.418(8) | 0.03(1) |
| | 1.214 | 0.500 | 0.502(3) | 0.506(8) | 0.03(1) |
| Improved (Landau) | 0.650 | 0.276 | 0.277(11) | 0.269(22) | 0.06(1) |
| | 0.795 | 0.333 | 0.335(4) | 0.330(9) | 0.04(1) |
| | 0.905 | 0.409 | 0.408(8) | 0.402(12) | 0.03(1) |
| Wilson | 1.950 | 0.250 | 0.189(2) | 0.183(7) | 0.19(1) |
| | 2.000 | 0.250 | 0.200(5) | 0.214(13) | 0.15(1) |
| | 2.140 | 0.333 | 0.267(4) | 0.271(7) | 0.11(1) |
| | 2.243 | 0.400 | 0.338(6) | 0.335(16) | 0.07(1) |
| | 2.300 | 0.500 | 0.428(3) | 0.419(9) | 0.06(1) |
| | 2.400 | 1. | | | 0.04(1) |

TABLE III. Measured anisotropies $(a_t/a_s)_{\text{phys}}$ compared to the input anisotropies ξ for the three actions. Each anisotropy was measured twice, using two different radii R_1 for the subtraction, with fixed $R_s = 2a_s$ (see Eq. (20)). The errors ΔV in the off-axis potential are also given.

| Action | β | a_s (fm) | $m_{0+}/\sqrt{\sigma}$ | $m_{2+}/\sqrt{\sigma}$ |
|-------------------------|---------|------------|------------------------|------------------------|
| Improved (Plaquette) | 0.848 | 0.366(1) | 3.49(7) | 4.4(7) |
| | 0.981 | 0.298(1) | 3.41(6) | 5.6(3) |
| | 1.114 | 0.238(1) | 3.55(5) | 5.9(1) |
| | 1.214 | 0.202(2) | 3.59(7) | 5.8(2) |
| Improved (Landau) | 0.650 | 0.384(2) | 3.74(5) | 5.7(1) |
| | 0.795 | 0.304(1) | 3.58(7) | 5.8(13) |
| | 0.905 | 0.244(1) | 3.72(8) | 5.7(5) |
| Wilson | 1.950 | 0.393(2) | 3.17(7) | 5.0(1) |
| | 2.000 | 0.355(2) | 3.10(5) | 5.1(1) |
| | 2.140 | 0.308(2) | 2.96(5) | 5.4(1) |
| | 2.243 | 0.232(2) | 3.05(6) | 5.6(1) |
| | 2.300 | 0.203(1) | 3.14(7) | 5.8(5) |
| | 2.400 | 0.128(2) | 3.52(11) | 5.8(2) |

TABLE IV. Scalar and tensor glueball masses from anisotropic lattices.

FIGURES

FIG. 1. Static quark potentials on isotropic lattices: (a) plaquette-improved action with $\beta_P = 0.730$; (b) mean link-improved action with $\beta_L = 0.550$; and (c) Wilson action with $\beta_W = 1.700$. Linear plus Coulomb fits to the on-axis potentials are shown as the solid lines.

FIG. 2. Effective potential at $R = a$ on the isotropic tadpole-improved lattice with $\beta_P = 0.730$.

FIG. 3. Effective mass plot for the scalar glueball on the isotropic tadpole-improved lattice with $\beta_P = 0.935$.

FIG. 4. Static quark potentials on anisotropic lattices, computed from Wilson loops W_{xt} (\bullet) and W_{xy} (\square). The potentials in lattice units obtained from W_{xt} have been rescaled by the input anisotropy, and the potentials have been shifted by additive constants in order to set $a_s V(R = a_s) = 1$. Linear plus Coulomb fits to the W_{xt} on-axis data are shown as the solid lines. Results are shown for (a) the plaquette-improved action at $\beta_P = 0.848$; (b) the mean link-improved action at $\beta_L = 0.650$; (c) the Wilson action, at $\beta_W = 1.950$.

FIG. 5. Effective mass plots for (a) scalar and (b) tensor glueballs on the anisotropic lattice with mean link improvement at $\beta_L = 0.795$. The result of a single exponential fit to the scalar glueball is shown as the solid line, with dotted lines showing the estimated error.

FIG. 6. Scalar glueball mass versus spatial lattice spacing squared. Data is shown for: the mean link-improved action (\blacksquare); the plaquette-improved action (\bullet); and from the Wilson action simulations done here (\circ). The result of a simulation with an adhoc change to the coefficients of the rectangle terms in the improved action, described in the text, is also shown (\triangle). We also include results from Wilson action simulations reported in Ref. [29] (\times). The star shows the results of an $a \rightarrow 0$ extrapolation of published Wilson action data [30].

FIG. 7. Tensor glueball mass versus lattice spacing squared. The plotting symbols are the same as in Fig. 7.

Figure 1a

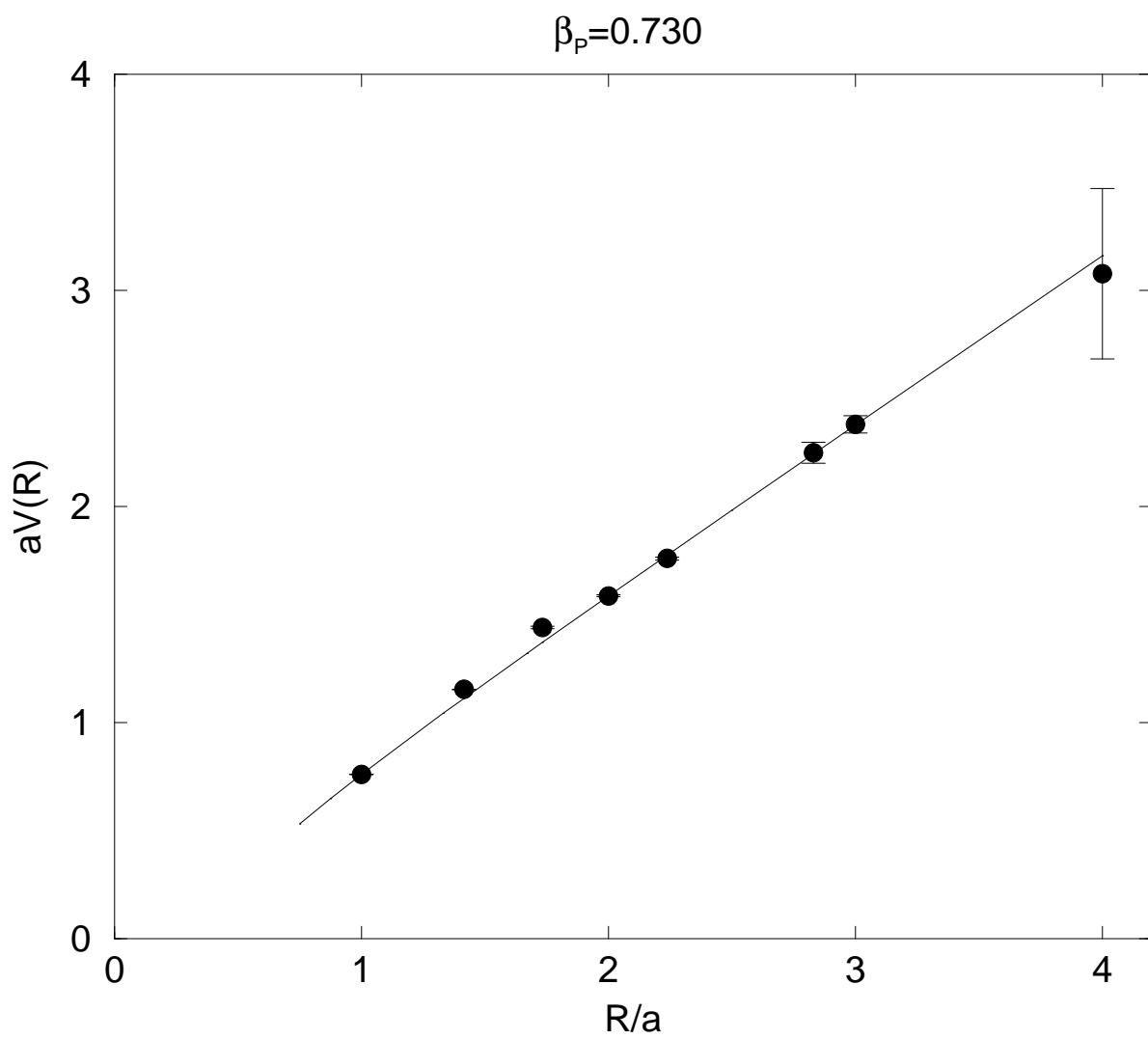


Figure 1b

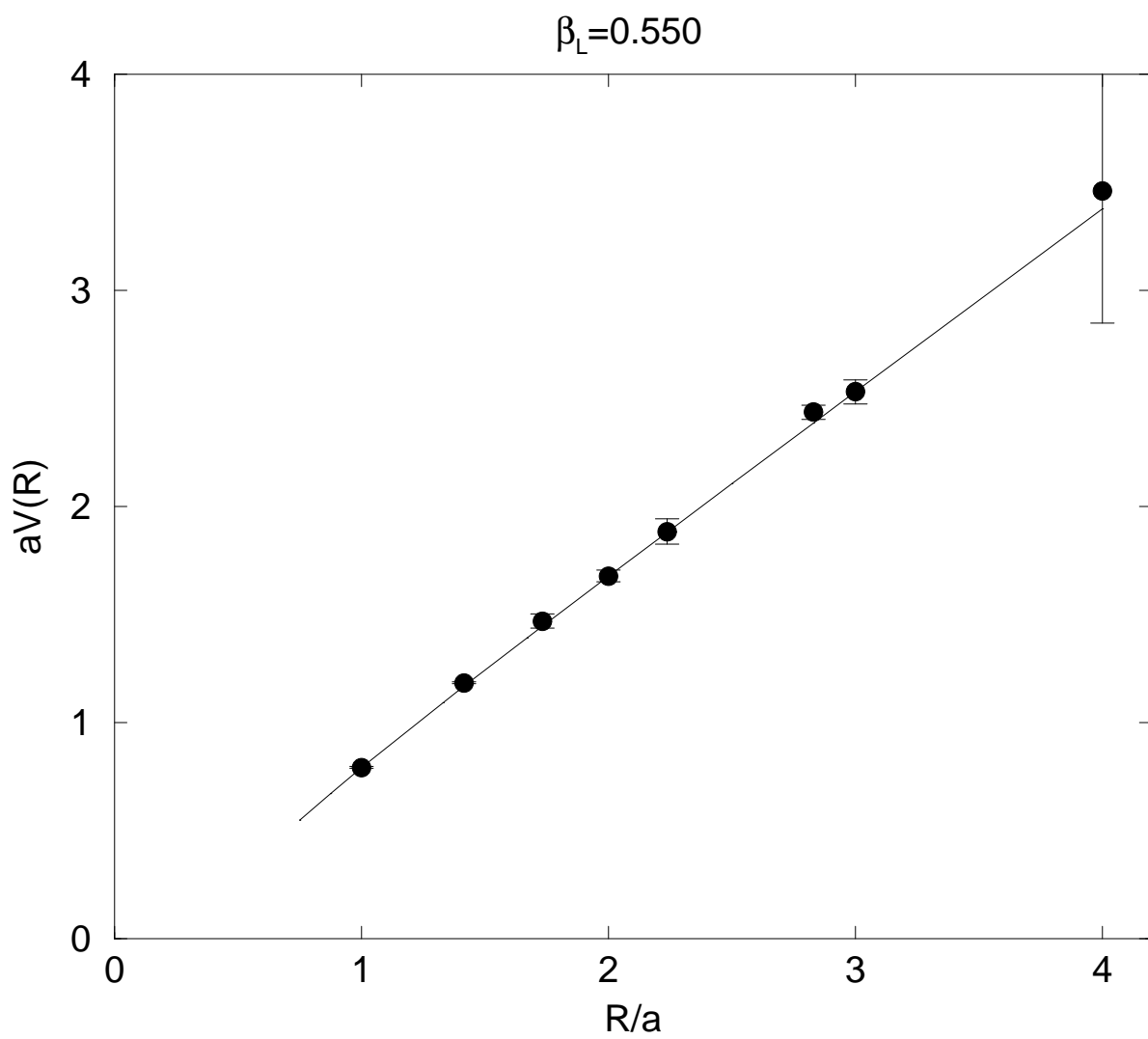


Figure 1c

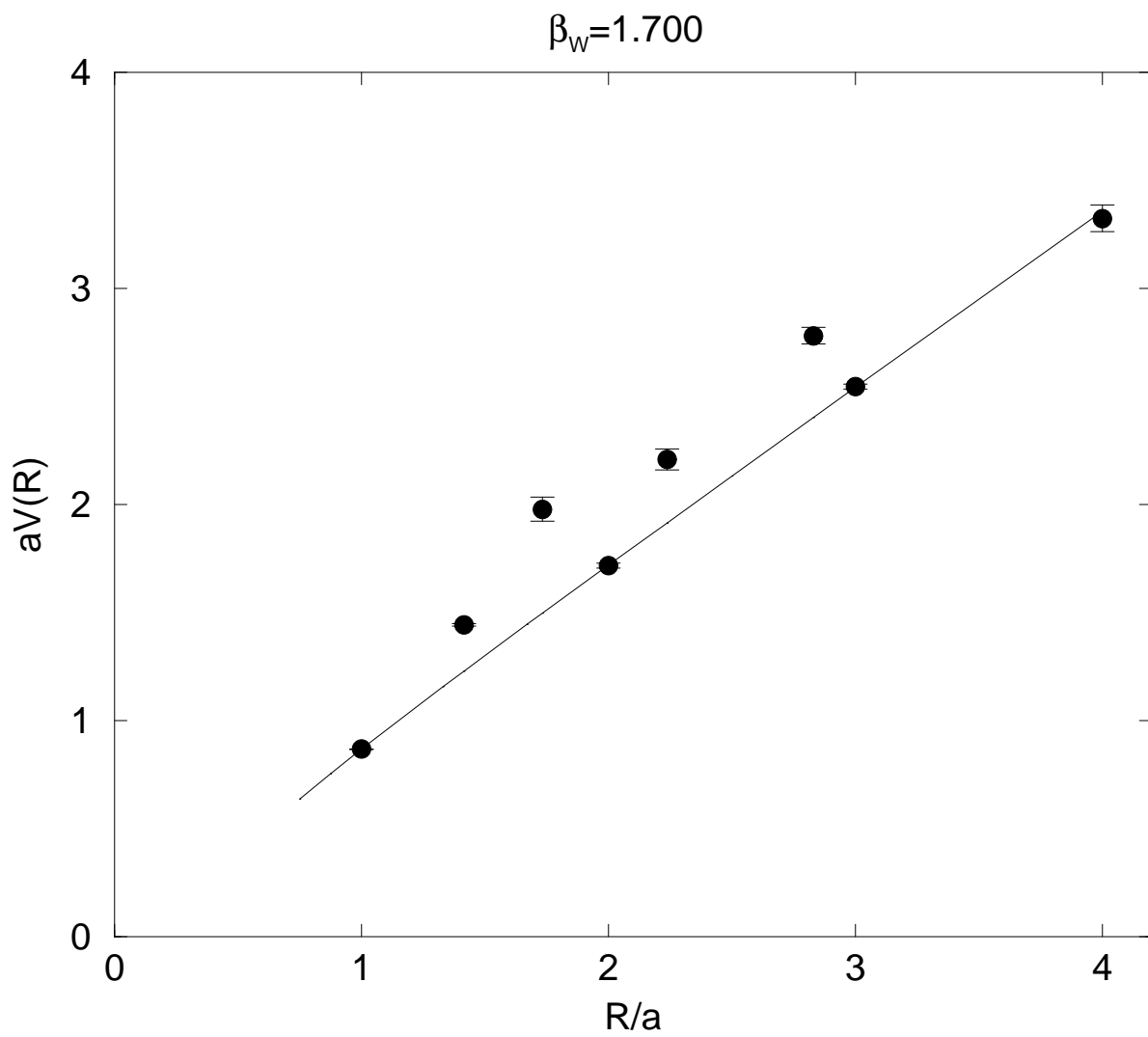


Figure 2

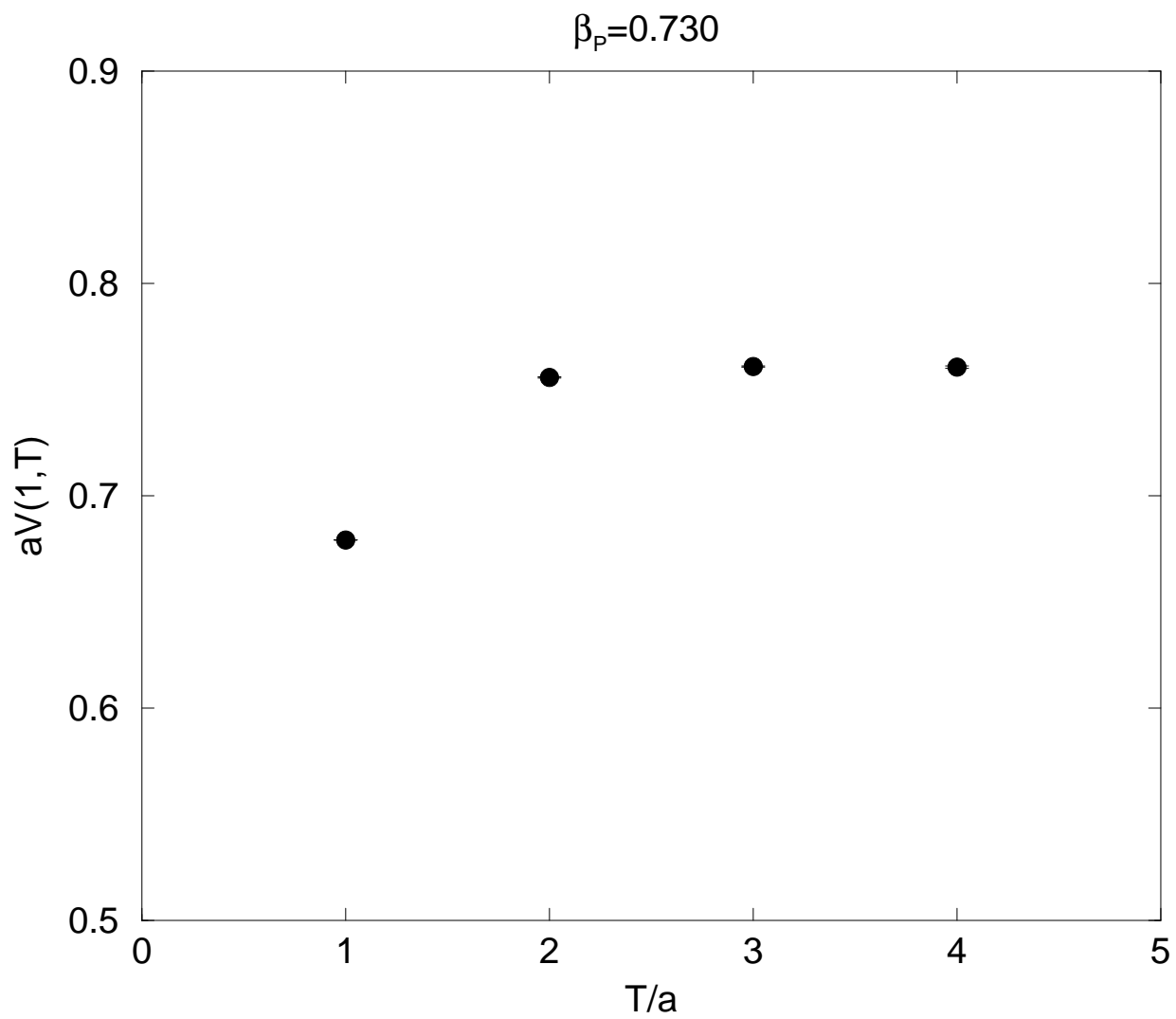


Figure 3

$\beta_p = 0.935$

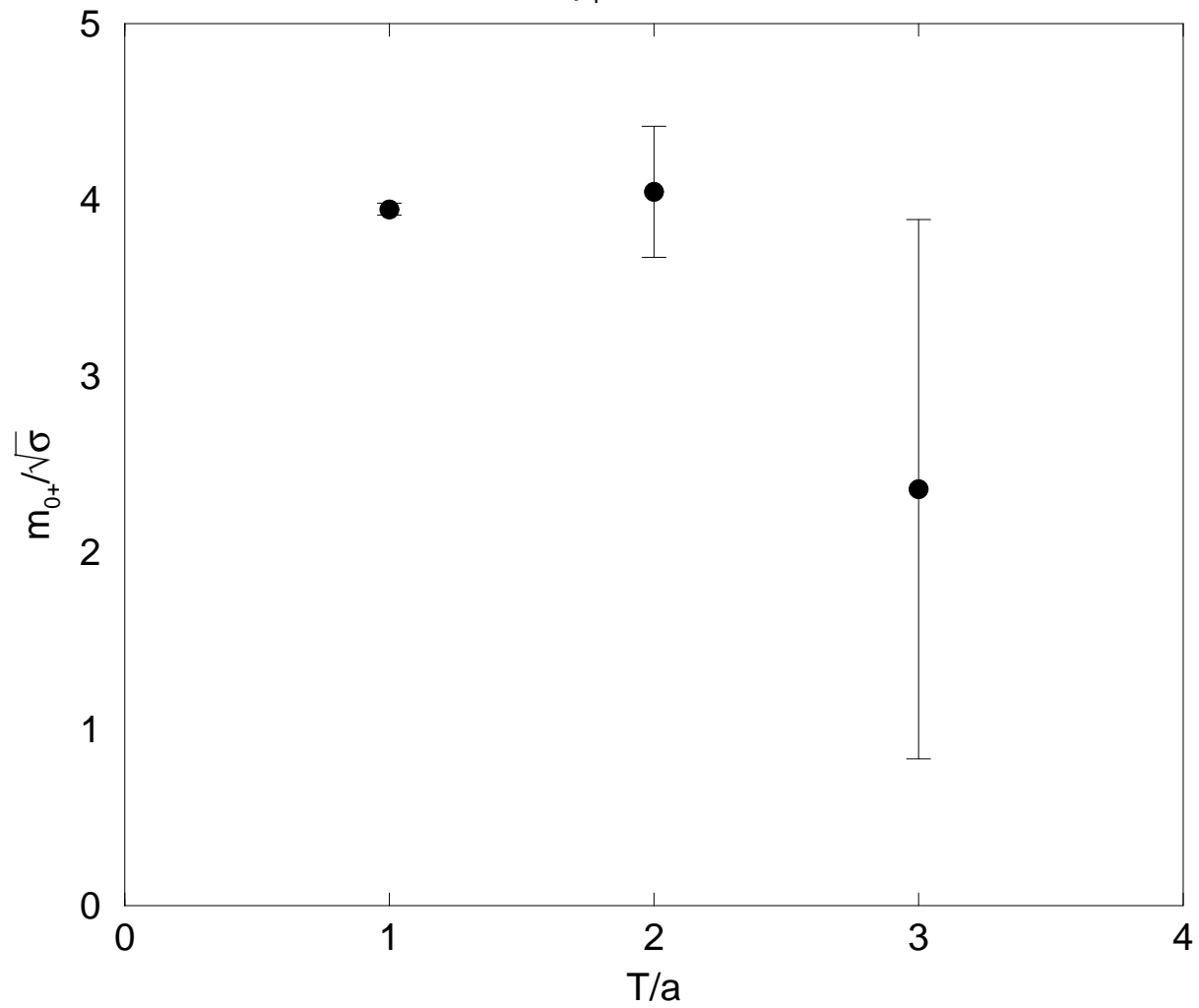


Figure 4a

$\beta_p = 0.848$

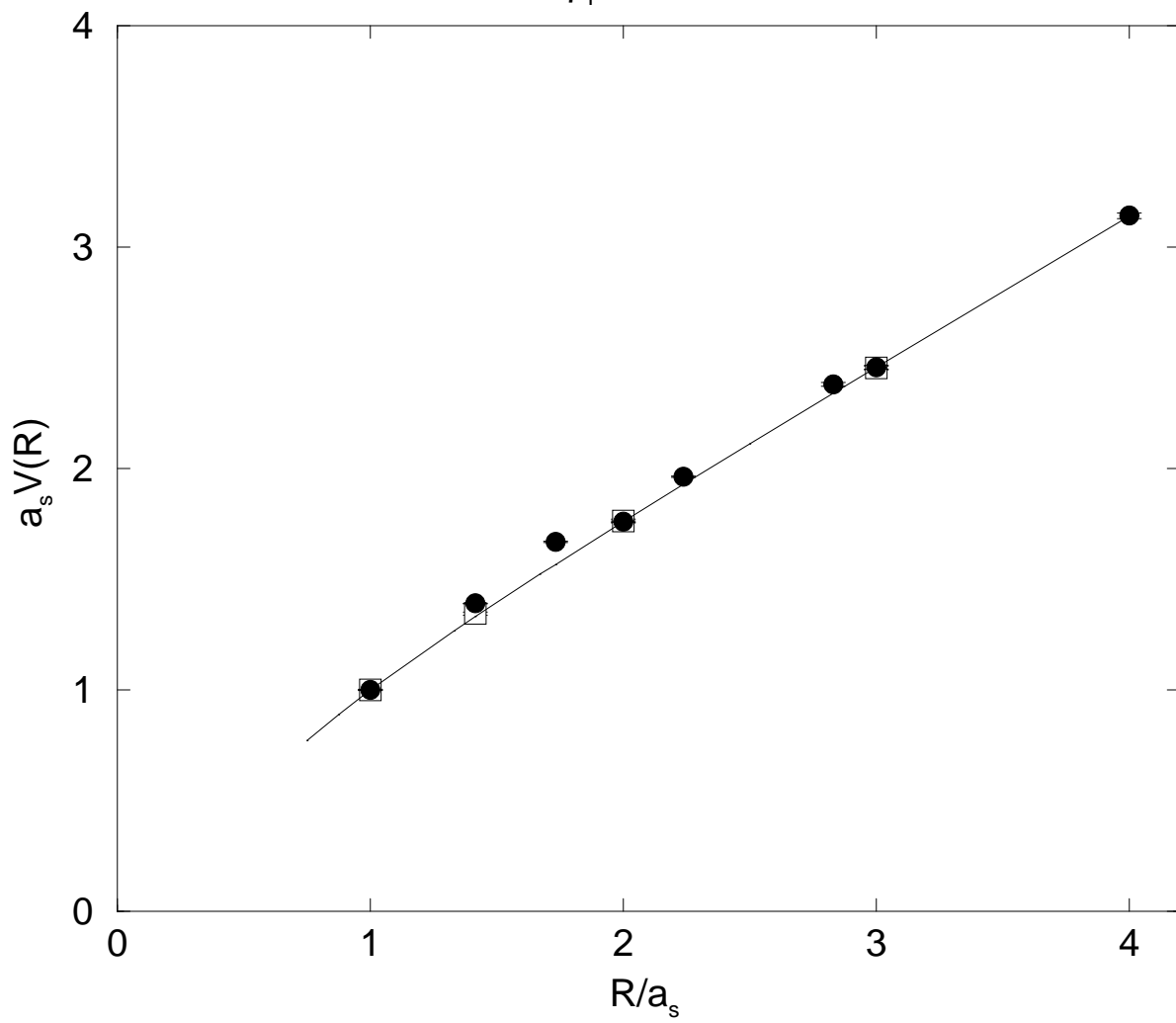


Figure 4b

$\beta_L = 0.650$

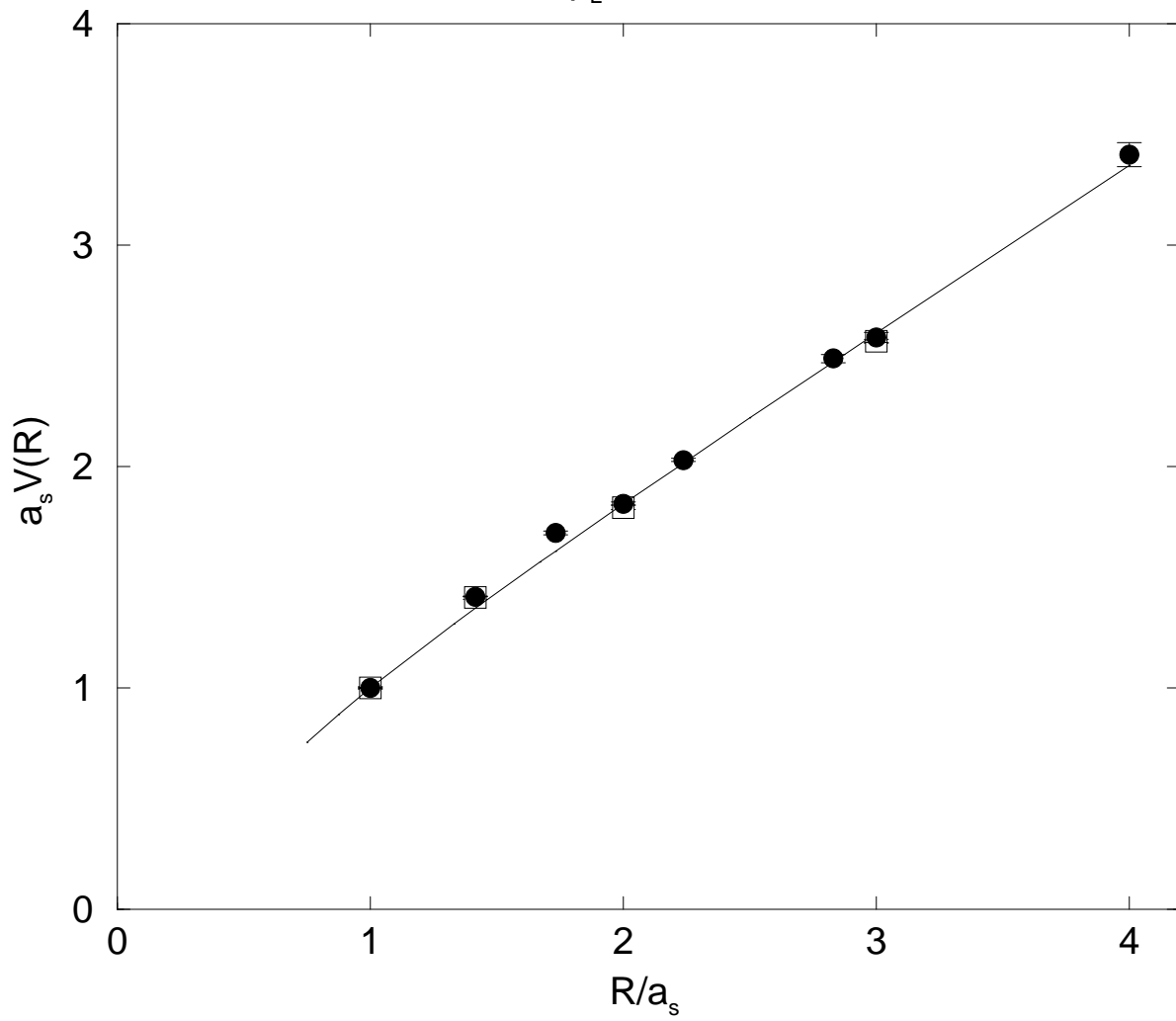


Figure 4c

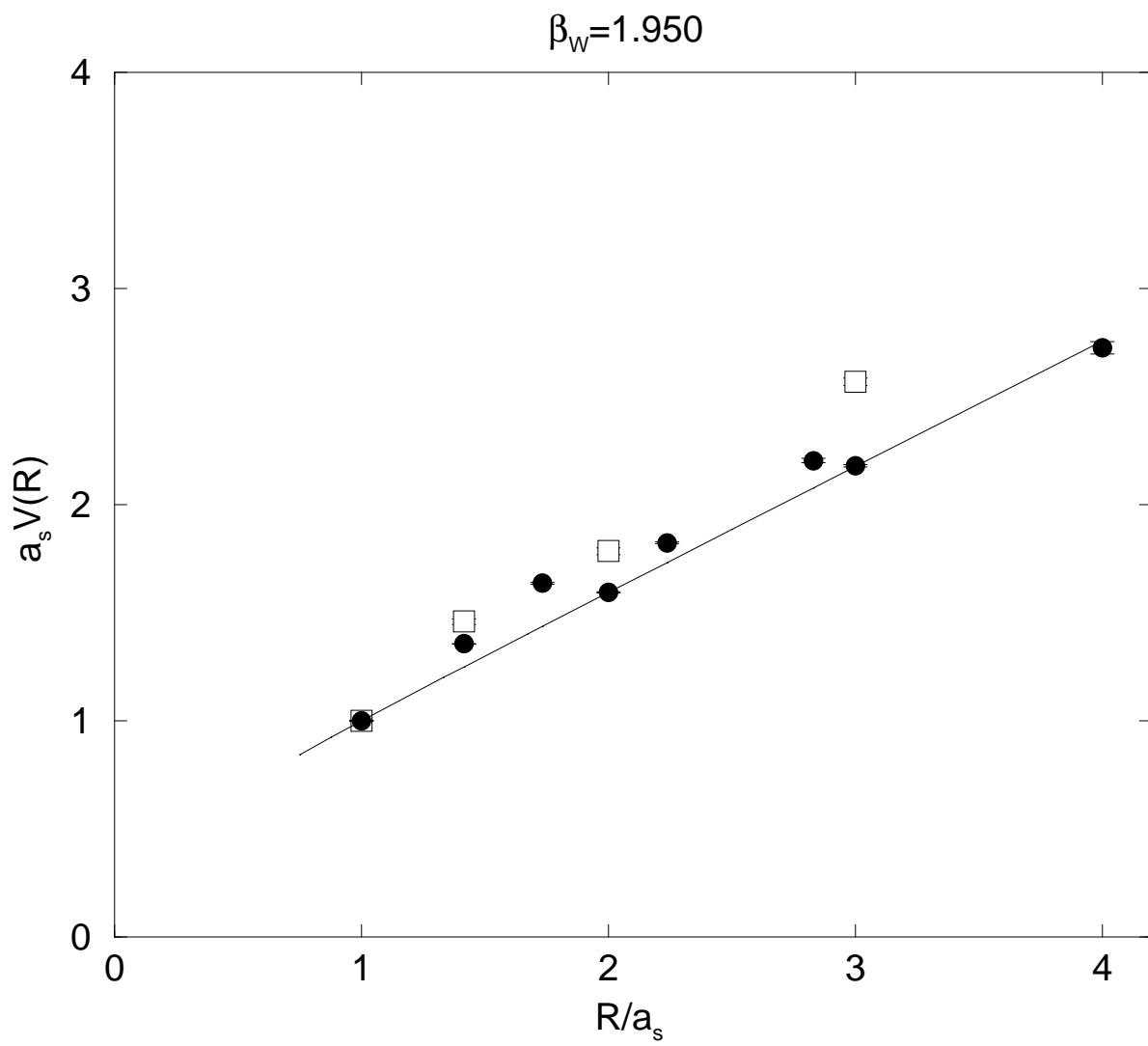


Figure 5a

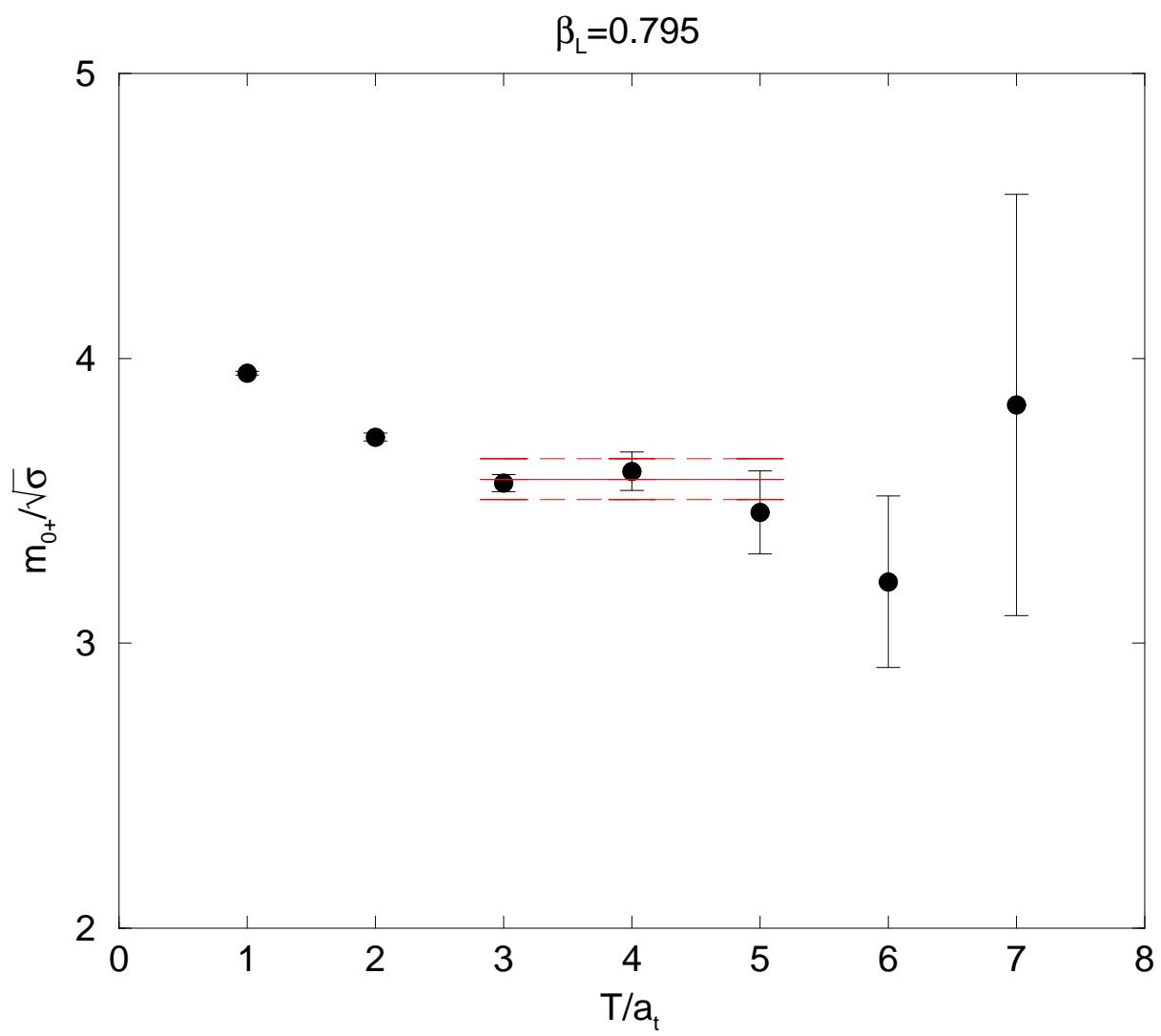


Figure 5b

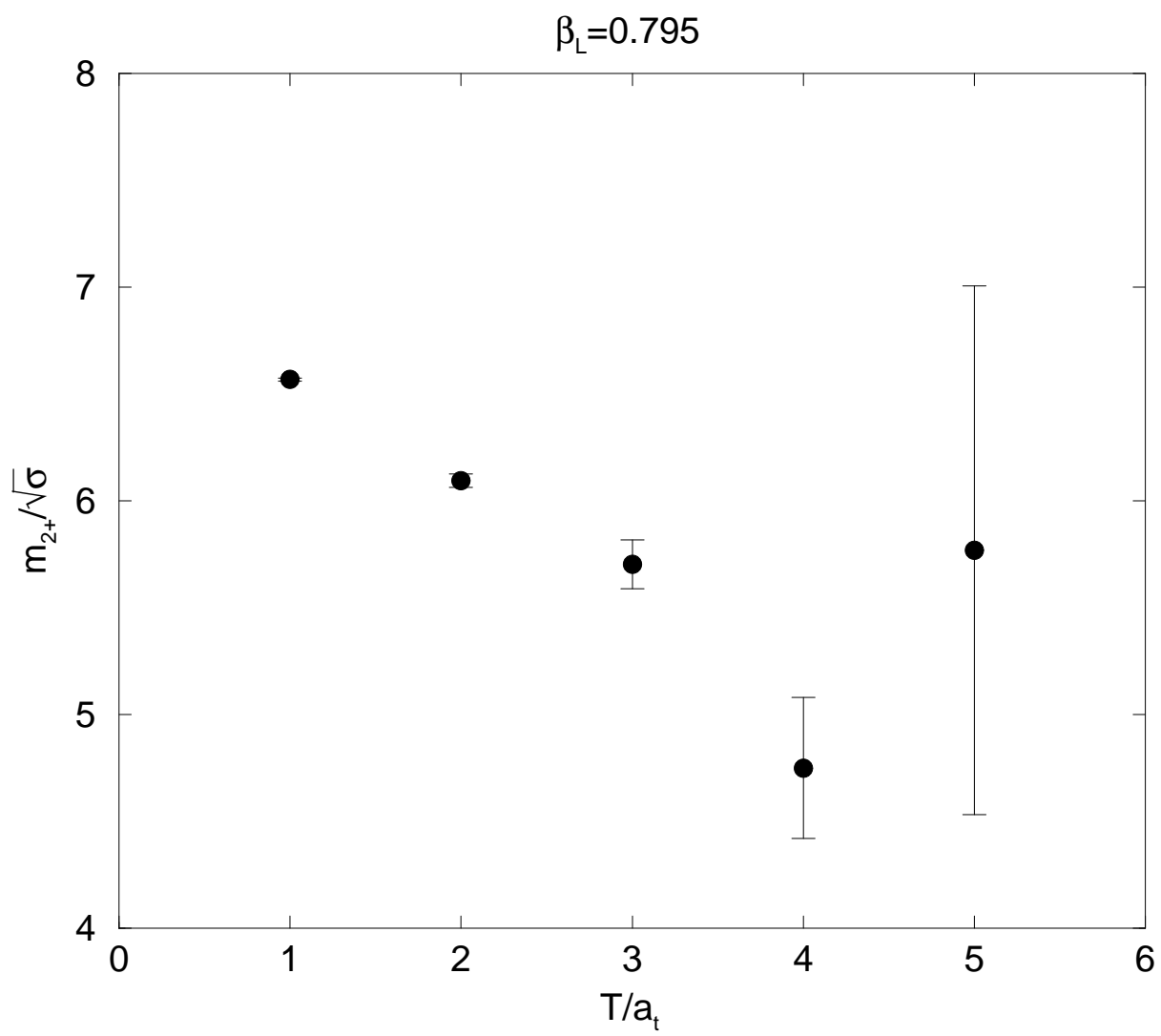


Figure 6

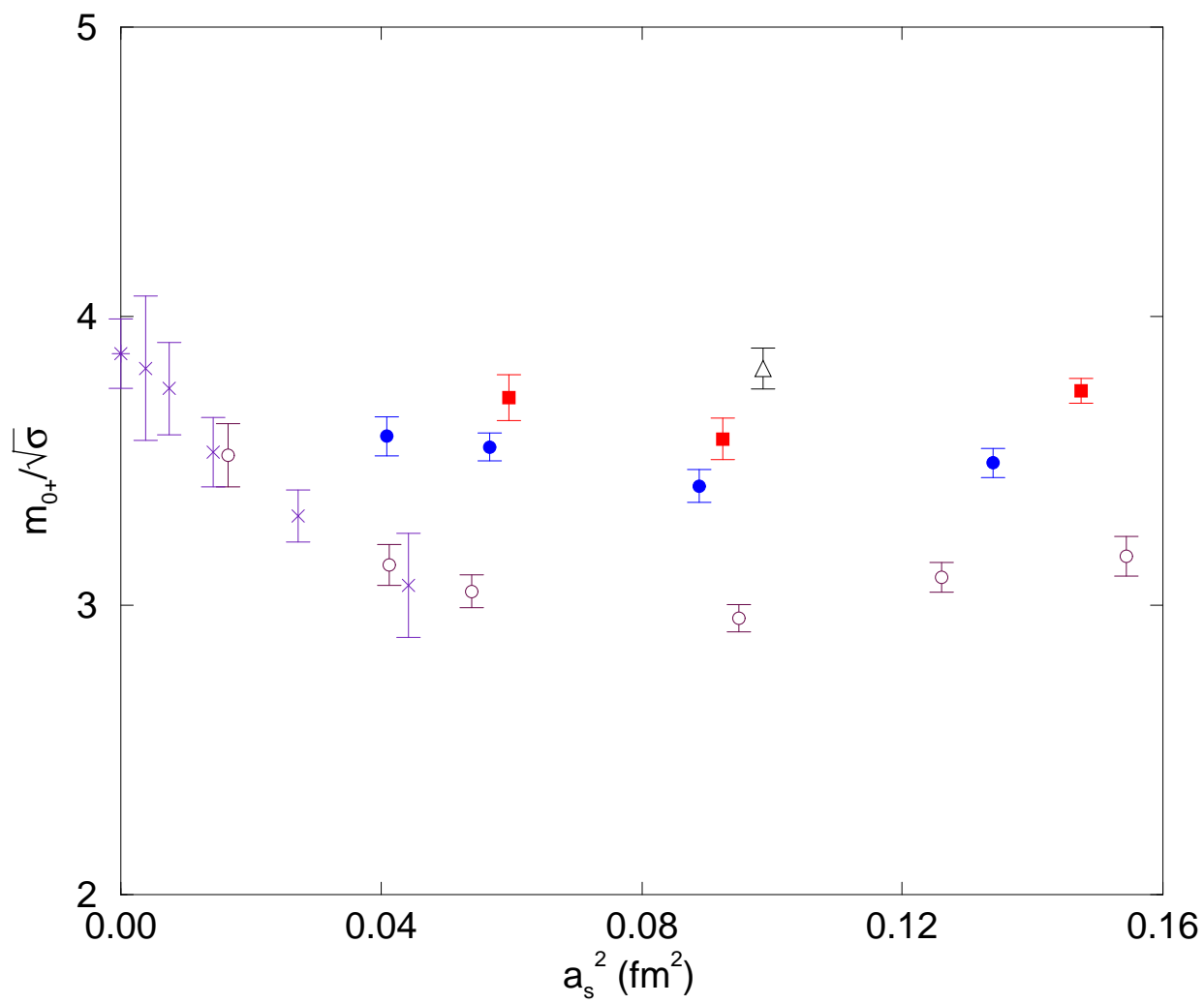


Figure 7

